

# MEMS OPTOMECHANICAL ACCELEROMETRY STANDARDS

Felipe Guzmán Cervantes<sup>1,2</sup>, Yiliang Bao<sup>1</sup>, Jason J. Gorman<sup>1</sup>, John R. Lawall<sup>1</sup>,  
Jacob M. Taylor<sup>1,2</sup>, and Thomas W. LeBrun<sup>1</sup>

<sup>1</sup>National Institute of Standards and Technology, Gaithersburg, MD 20899, USA

<sup>2</sup>Joint Quantum Institute, University of Maryland, College Park, MD 20742, USA

## INTRODUCTION

Primary accelerometer calibrations are often performed at National Metrology Institutes (NMI)[1], where the test units are mounted onto interferometrically-interrogated reference shaker systems[2, 3, 4], which typically reach relative uncertainties of the order of  $10^{-2}$ – $10^{-3}$ . Reference accelerometers that have been calibrated at primary facilities, are used, in turn, to calibrate additional devices using back-to-back measurements. This latter approach, however, often results in reduced performance and higher uncertainty. In addition, there is an increasing need in industry, aerospace and defense applications for cost-effective in-the-field calibrations that minimize down time and drift of reference systems.

As part of the research funding initiative from the National Institute of Standards and Technology (NIST), NIST-on-a-Chip, we are developing portable chip-based accelerometers that incorporate displacement measurement interferometry to produce NMI-grade measurements that are directly traceable to the International System of Units (SI). The device design further detailed below, will allow both cost-effective production for wide deployment due its compatibility with MEMS semiconductor fabrication, and self-monitoring to ensure the specified measurement uncertainty over the certified lifetime of the device.

In addition to the improvements in acceleration metrology and calibrations, this research will greatly impact enabling technologies, particularly for inertial navigation systems. Current performance challenges, such as bias and scale factor stability, are tied to the uncertainty of the system, which will be directly addressed by this work. Similarly, research in seismology, ground and space-based geodesy, which base their observations in great extent to a traceable acceleration measurement, will benefit from such highly compact devices of significantly higher sensitivity and accuracy.

This article presents the sensor and measurement concept under study and preliminary results on the chip-based micro-optomechanical device fabrication and laser-interferometric results.

## OPTOMECHANICAL ACCELEROMETER

Our concept for MEMS optomechanical acceleration standards is based on a micromechanical resonator that vibrates out of plane and incorporates a plano-concave Fabry-Pérot (FP) cavity to read out the motion of the accelerometer test mass, as shown in Figure 1. Furthermore, an additional stage can be added to the back side of the test mass for capacitive sensing and electrostatic force rebalance.

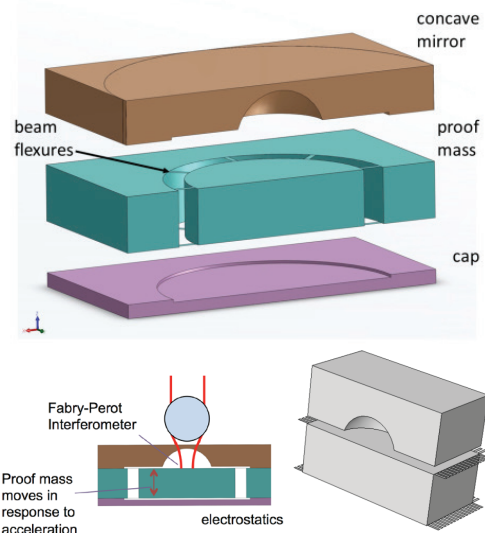


FIGURE 1. Schematics of the Si MEMS optomechanical accelerometer standard, incorporating a plano-concave Fabry-Pérot cavity.

Assuming a simple harmonic oscillator response for the mechanical resonator, acceleration can be obtained from a direct displacement measurement of the test mass by

$$\frac{X(\omega)}{A(\omega)} = -\frac{1}{\omega_0^2 - \omega^2 + i\frac{\omega_0}{Q}\omega}, \quad (1)$$

where  $X(\omega)$  is the relative displacement given an

input acceleration  $A(\omega)$  at an angular frequency  $\omega$ , with a harmonic oscillator response of the mechanics determined by its natural frequency  $\omega_o$  and quality factor  $Q$ .

Presently, we strive to achieve a relative measurement uncertainty below  $10^{-3}$  in a dynamic range of  $1\text{ mg}-1\text{ g}$  over an observation bandwidth of  $1\text{ Hz}-20\text{ kHz}$ . The performance of accelerometers is commonly specified in units of  $g$ , which is defined as  $9.80665\text{ m/s}^2$ , referred to the SI. By integrating a laser interferometer into the system it is possible to measure the test mass displacement in terms of an optical frequency/wavelength standard.

In addition, as shown in Equation 1, a complete system identification consists of only two parameters, namely the resonance frequency  $\omega_o$  and quality factor  $Q$ . Therefore, this knowledge is sufficient to compute acceleration from a displacement measurement with no additional information, assuming the accelerometer exhibits a linear response with a measurable damping mechanism. These parameters can also be measured and calibrated with respect to frequency standards, which provides traceability to the SI, and enables verification of device performance in the field.

## DEVICE NANOFABRICATION

### Hemispherical Mirrors

An outline of the nanofabrication process we have developed to fabricate the concave mirrors is shown in Figure 2. As a base substrate

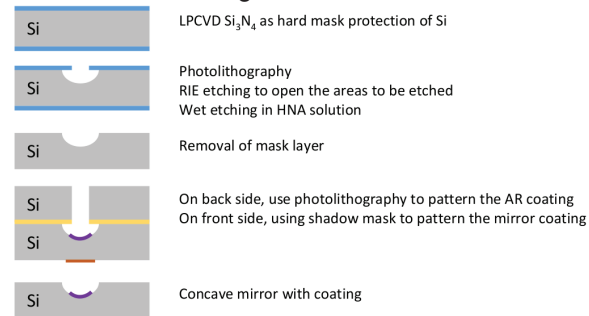


FIGURE 2. Outline of nanofabrication process of silicon hemispherical mirrors.

we utilize a silicon (Si) wafer with a thickness of  $500\text{ }\mu\text{m}$ , and deposit a  $300\text{ nm}$  silicon nitride ( $\text{Si}_3\text{N}_4$ ) layer as a hard mask on top of it by applying a low-pressure chemical vapor deposition (LPCVD). The wafer is then patterned lithograph-

ically using photoresist SPR 220.3, and this pattern is then transferred to the  $\text{Si}_3\text{N}_4$  hard mask by reactive ion etching (RIE). The hemispherical concavity results from a wet etching process using a HNA solution of  $\text{HF}:\text{HNO}_3:\text{CH}_3\text{COOH}$  with a ratio of 9:75:30 at room temperature. Subsequently, the  $\text{Si}_3\text{N}_4$  hard mask is removed by phosphoric acid and the wafer is then sent for a final RCA cleaning. Once the mirror geometry is completed in the nanofabrication process, the optical properties of the final micro-optical components are defined by applying an anti-reflection coating to the back side of the wafer to reduce stray beams and undesired optical etaloning. Additionally, a typically high-reflectivity dielectric coating is applied to the front side of the wafer to define the input mirror of a high finesse optical cavity. Figure 3 shows scanning electron microscopy (SEM) images and post-processed white light interferometry (WLI) measurements, revealing a mirror geometry with a radius of curvature of typically  $300\text{ }\mu\text{m}$ , a depth of  $220\text{ }\mu\text{m}$ , an aperture diameter of  $560\text{ }\mu\text{m}$  and surface roughness of approximately  $1\text{ nm}_{\text{rms}}$ .

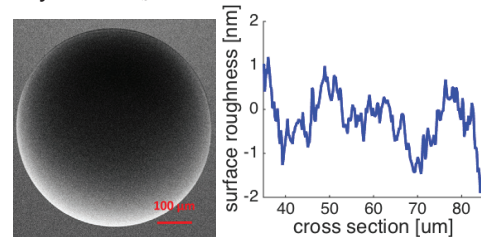


FIGURE 3. SEM and post-processed WLI measurements of hemispherical mirrors with a surface roughness of  $1\text{ nm}_{\text{rms}}$ .

### Mechanical Oscillator

The nanofabrication process developed for our mechanical resonators is outlined in Figure 4.

Similar to the case of the hemispherical mirrors, we use a  $500\text{ }\mu\text{m}$  thick double-sided polished silicon wafer, and create a  $3\text{ }\mu\text{m}$  deep spacer using HNA etching with a  $\text{Si}_3\text{N}_4$  hard mask. The layer to produce the released-beam resonator pattern is achieved via  $\text{Si}_3\text{N}_4$  LPCVD. Following the coating of the mirror using a lift-off process, a  $1\text{ }\mu\text{m}$  low temperature oxide (LTO) layer was deposited via LPCVD to serve as a hard mask for subsequent wet etching. The wafer is then patterned lithographically on both sides with photoresist SPR 220.7 ( $10\text{ }\mu\text{m}$  thickness) and transferred to the  $\text{Si}_3\text{N}_4$  hard mask by RIE. Lastly, deep reactive ion etching (DRIE) is conducted to etch through the silicon wafer, and isotropic KOH silicon etching is

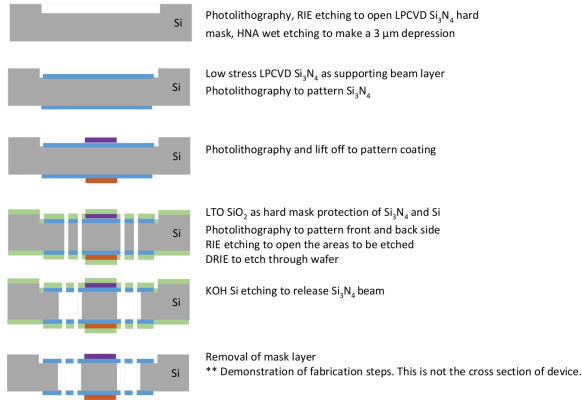


FIGURE 4. Outline of nanofabrication process of silicon mechanical resonators.

employed to release the silicon nitride beams with the oxide hard mask, which is then removed as a final step. Figure 5 shows images of the released beams and mass of our mechanical oscillator.

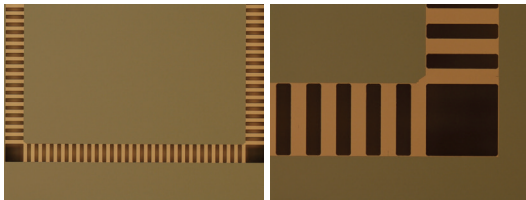


FIGURE 5. Images of the released beams and mass of our mechanical oscillator.

### OPTICAL DETECTION SCHEME

In order to build an integrated high sensitivity optical sensor, a plane-concave Fabry-Pérot cavity is assembled between the flat surface of the moving test mass and a hemispherical input mirror with a radius of curvature around  $300\ \mu\text{m}$ . The depth of the concave mirror is about  $220\ \mu\text{m}$ . Typical cavity lengths between  $230\text{--}270\ \mu\text{m}$  are currently being tested in order to maintain a stable optical cavity, yielding free spectral ranges around  $600\ \text{GHz}$ . Moderate finesse ( $\mathcal{F}$ ) levels in the order of  $1000$  combined with such a large FSR make it challenging to reliably implement conventional AC detection and cavity-lock schemes, such as Pound-Drever-Hall, due to the wide cavity linewidths involved and the necessary high modulation frequencies. Feasible alternatives can be implemented by applying deep dither modulations to the cavity length or laser frequency. It is our goal to develop cavities of finesse levels higher than  $10^4$  in order to accomplish narrow linewidths that enable both, robust detection and locks as well as

significantly higher sensitivity.

An additional challenge resulting from such short cavity lengths is posed on both, the laser system and the cavity length actuation. Due to the large FSR, a dynamic range of several  $10\text{s}$  to  $100\text{s}$  of  $\text{GHz}$  may be required to tune the laser frequency to the cavity resonance. Presently, we utilized a largely tunable telecom laser with a wavelength nominally around  $\lambda = 1550\ \text{nm}$  and tunable range of  $50\ \text{nm}$ . We operate at moderate optical power levels of approximately  $1\ \text{mW}$ .

The optical output of a Fabry-Pérot cavity in reflection, as a function of the laser wavelength  $\lambda$  can be modeled by the Airy function, describing the signal  $V(L, \lambda)$  measured at the photoreceiver[5]

$$V(L, \lambda) = v_o + \gamma \frac{(1 + R)^2}{2} \left[ \frac{1 - \cos\left(\frac{4\pi}{\lambda} L\right)}{1 + R^2 - 2R \cos\left(\frac{4\pi}{\lambda} L\right)} \right] \quad (2)$$

where  $L$  is the cavity length,  $\lambda$  is the laser wavelength,  $R$  is the net reflectivity of the cavity mirrors,  $\gamma$  is the signal visibility, and  $v_o$  is an offset. Given the wide tunability range of our laser, it is possible to measure a few FSR of the cavity and thus directly measure the optical cavity length  $L$  as,

$$L = \frac{c}{2\text{FSR}} \quad (3)$$

High sensitivity displacement measurements at levels of  $10^{-14}\ \text{m}/\sqrt{\text{Hz}}$  and  $10^{-16}\ \text{m}/\sqrt{\text{Hz}}$  have been demonstrated in similar micro-optomechanical systems with low[5] and high[6] finesse fiber-optic cavities, respectively. Figure 6 shows the different responses for low ( $\mathcal{F} = 2$ ) and high ( $\mathcal{F} = 1000$ ) finesse silicon cavities with a length of  $250\ \mu\text{m}$ .

We have been able to demonstrate stable cavities of modest finesse with our nanofabricated silicon mirrors. Figure 7 shows the response of a  $170\ \mu\text{m}$  long cavity with a modest finesse of  $14$ , which yields a FSR of  $890\ \text{GHz}$  and a cavity linewidth of  $64\ \text{GHz}$ .

Furthermore, in spite of such large cavity linewidths, we have demonstrated closed-loop locked operation of these cavities by applying a low frequency deep modulation to the cavity length at  $1\ \text{kHz}$  via a piezo-electric transducer. A data chart illustrating this operation mode is presented in Figure 8.

A fully assembled MEMS optomechanical accelerometer is in progress. It is expected that

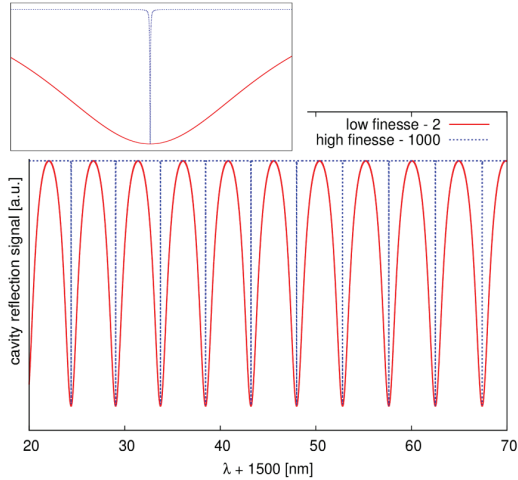


FIGURE 6. Response of silicon cavities with a length of  $250\ \mu\text{m}$  and finesse levels of 2 in red, and 1000 in blue.

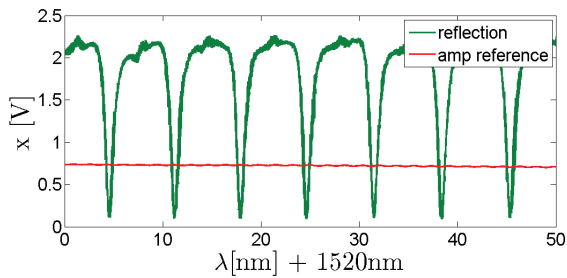


FIGURE 7. Response of a  $170\ \mu\text{m}$  long cavity using our hemispherical Si mirrors with a gold coating.

a first acceleration measurement with these devices can be demonstrated within the next few months. Moreover, our current data and cavity responses indicate that it will be possible to achieve the targeted displacement resolutions at levels of  $10^{-15}\ \text{m}/\sqrt{\text{Hz}}$ , by comparison to the results published on similar devices[5, 6].

Hence, we fully anticipate to meet our target accuracy below  $10^{-3}$  for acceleration measurements with portable chip-based optomechanical standards.

## DISCLAIMER

Certain commercial equipment, instruments, processes or materials are identified in this paper for completeness. Such identification does not imply a recommendation or endorsement by the National Institute of Standards and Technology.

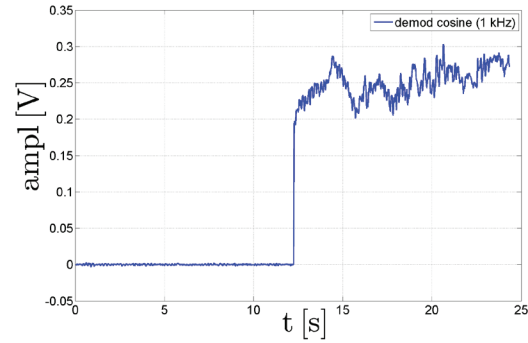


FIGURE 8. Data chart illustrating a 1 kHz low-frequency closed-loop cavity lock with a cavity linewidth of 64 GHz.

## ACKNOWLEDGEMENTS

The authors thank Jon R. Pratt and John A. Kramar for useful discussions. This research is supported by the NIST-on-a-Chip initiative. Research performed in part at the NIST Center for Nanoscale Science and Technology Nanofab.

## REFERENCES

- [1] Donald Clarke Robinson, MR Serbyn, and BF Payne. A description of NBS calibration services in mechanical vibration and shock. US Department of Commerce, National Bureau of Standards, 1987.
- [2] Gustavo P. Ripper, Ronaldo S. Dias, and Guilherme A. Garcia. Primary accelerometer calibration problems due to vibration exciters. Measurement, 42(9):1363–1369, 2009. Concerning Foundational Concepts of Measurement Special Issue Section.
- [3] Hans-Jürgen von Martens, Alfred Link, Hans-Joachim Schlaak, Angelika Taeubner, Wolfgang Wabinski, and Uwe Goebel. Recent advances in vibration and shock measurements and calibrations using laser interferometry. Proc. SPIE, 5503:119, 2004.
- [4] Hans-Jürgen von Martens. Evaluation of measurement uncertainty in calibrations of laser vibrometers. 1600:123–142, 2014.
- [5] Oliver Gerberding, Felipe Guzmán Cervantes, John Melcher, Jon Pratt, Jacob Taylor. Optomechanical reference accelerometer. arXiv.org:1504.01055, submitted to Metrologia, 2015.
- [6] Felipe Guzmán Cervantes, Lee Kumanchik, Jon Pratt, and Jacob M. Taylor. High sensitivity optomechanical reference accelerometer over 10 kHz. Applied Physics Letters, 104(22):221111, 2014.